Characterisation Study on Engineered Biochar from Agro-Waste to Be Used as Potential Biosorbents

Sinovuyo Cebo Amahle Kraai^{*1}, Thembisile Monama², Sudesh Rathilal¹, Emmanuel Tetteh¹

Abstract— The continuous growth of the human population associated with industrial activities has contaminated water with heavy metals. The growth in human population also translates into an increase in agricultural activities, which leads to agricultural waste landfills that have long-term negative effects on the environment. In essence, the presence of non-biodegradable heavy metals in industrial effluent poses serious health risks to humans and other living organisms. Therefore, removing heavy metals from industrial wastewater must be a high priority.

This study aims to ensure agro-waste management by studying the potential of engineered biochar from agro-waste to be used as biosorbents. Considering that agro-waste is generally considered as waste, it would be an economical biosorbent. The biochar was synthesized from agro waste (banana peels, orange peels, and sugarcane bagasse) through the calcination process. Then the produced biochar was characterized using Scanning Electron Microscopy (SEM), Fourier Transform Infrared Spectroscopy (FTIR), and X-Ray Diffraction (XRD) to study the potential it has for being used as a biosorbent for heavy metal removal from wastewater. From the SEM results for all biowaste material, it was observed that as the calcination temperature increases so does the porousness increase, meaning increased adsorption sites. For the FTIR results, the most common functional groups observed in all agro-waste studied were O-H, and C=O groups (which generally show great affinity to heavy metals), especially for calcined temperatures from 300 to 500 0C. The XRD results showed that biochar calcined at 400 and 500 0C had the fraction $2\theta = 230$ which corresponded with about 10 crystal planes, indicating high crystal content at these high calcination temperatures. The outcomes of this research may lead to the enhancement of the sustainability of agro-waste utilization in wastewater treatment through biosorption.

Keywords - Agro-waste, Heavy Metals, Wastewater, Landfills.

I. INTRODUCTION

The rapid rise of human and industrial activities has led to an increase in the concentration of heavy metals found in wastewater and other water bodies. Heavy metals are a threat to human and environmental health. Some of the sources of heavy

¹Green Engineering Research Group, Department of Chemical Engineering, Steve Biko Campus Block S4 Level 1, Box 1334, Durban, 4000, South Africa ²University of Johannesburg, Postgraduate School of Engineering Management Faculty of Engineering & the Built Environment Green 10, Auckland Park Bunting Road Campus metals include, but not limited to, mining, tanneries, and metal plating [1]. The effluent from the mentioned industries tends to have large presence of heavy metals. Heavy metals contaminatewaterbodies through wastewater streams from industries whichpose harm to aquatic life and are later consumed by humans [2,3]. These heavy metals end up in the human food chain because of their ability to attach proteins, nucleic acids, small metabolites in living organisms [4]. Consequently these heavy metals pose serious health threat to plant, human and animal health because of their ability to bioaccumulate in their host's body [4].

A variety of conventional methods such as electro-dialysis, ionexchange, reverse osmosis, adsorption, and chemical precipitation have been proposed for the removal of heavy metals from industrial wastewater [5]. However, adsorption has been widely recognized as an efficient method of removing heavy metals due to its cost effectiveness, efficiency, and ecofriendliness [5-8]. Activated carbon is the most commonly used adsorbent for the adsorption process, but its high costs of fabrication often limits its application. Hence, there has been a rise in the proposal of the use of biowaste material as biosorbents (substitutes for activated carbon). The fact that they are readily available, require low cost for synthesizing, and do not generate secondary pollutants as much as activated carbon makes them a very attractive option to explore [7]. Biowaste materials which could be used as biosorbents include, but are not limited to, rice husk, banana peels, leaves, tree barks, orange peels, and sugarcane bagasse. However, this paper will focus on banana peels, orange peels, and sugarcane bagasse mainly because of their high presence in the KwaZulu-Natal province, South Africa [9, 10].

With this rise in the human population, the demand for agricultural activities has also risen exponentially as food is a necessity for everyone [11]. Thus leading to more landfills from agricultural waste disposal [11]. Agricultural waste products are produced in enormous quantities, since they have no financial value they are carelessly discarded thus becoming a burden to the environment [4]. Thus making the agricultural sector to be the amongst the most significant contributors in generating waste and uses valuable real estate as agricultural soils [4]. This brings rise to other environmental concerns such as land pollution and water pollution through rain rundowns. Open dumping of agricultural waste and byproducts causes environmental quality degradation due to contamination and clogging of water channels [12].

The objective of this paper is to study the potential of the utilization of valueless agro-waste as a biosorbent for

wastewater treatment. This will be achieved through characterizing the engineered biochar from agro-waste using SEM, FTIR, and XRD analysis technologies. The paper will only focus on the characterization of engineered biochar from agro-waste as potential biosorbents which could be used in biosorption technology. However, an application study of the engineered biochar in biosorption will be done on a separate paper.

To address the issues abovementioned this project will study the adsorption of these heavy metals from wastewater using engineered biochar from agro-waste (agricultural waste) as a potential solution. Studying this option as a potential solution would lead to the reduction of heavy metals in wastewater and agricultural waste management. The potential of this research is not to only solve environmental issues associated with the problem. The solution proposed may also add value to the seemingly valueless "waste products" of the agricultural sector. As the wastewater will be treated for reuse and the agro-waste will be converted into biochar rather than just being discarded in landfills.

The process that was used to prepare biochar is called, calcination. The calcination process is done by heating materials at high temperature and under deficit of oxygen presence to produce biochar and synthesis gas (syngas) [13]. Syngas is a versatile gas which is a crucial precursor in the synthesis of many chemicals and fuels, and it constitutes of carbon monoxide (CO) and hydrogen (H2) [14] [15].

II. MATERIALS AND METHODS

Orange and banana peels were collected from the Durban central fruit and vegetable market waste bins. Sugarcane bagasse was collected from one of the local sugar mills located in Durban, KwaZulu Natal, South Africa. After the collection of all the agro-wastes from their respective places they were then separately washed with tap water several times, then thereafter they were washed with deionized water three times. After washing they were dried at 105 0C for 24 hrs, using the heating incubator RHI series RHI shown in figure 1.

Thereafter, the dried agro-waste materials were separately crushed using a blender into powder form. The powder form was then poured into crucibles for calcination where they were calcined, at temperatures 300; and 500 0C to make biochar, using the Kiln Contracts lab kiln (see figure 1). However, some powdered agro-waste was not calcined. The uncalcined and calcined (at all the mentioned calcination temperatures) were then taken for characterization.

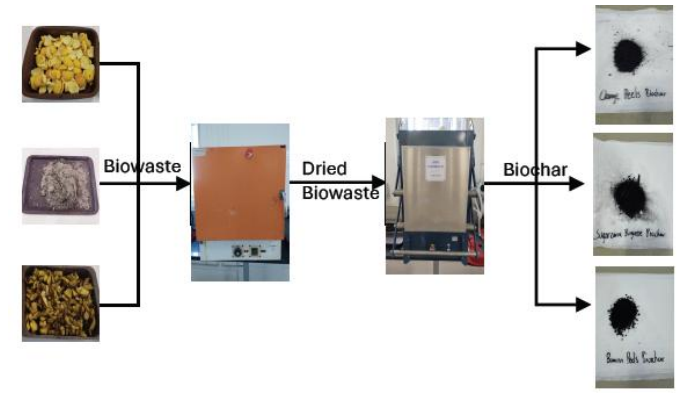


Fig. 1: Process flow diagram showing the production of biochar from biowaste

The biomaterials were characterised to determine their dominant surface functional groups, morphology, crystallographic structure, and surface area. The functional groups were determined using the Agilent Cary 630 Fourier transform infrared (FTIR) spectrometer. The morphology was determined using the TESCAN MIRA's 4th generation Scanning Electron Microscope (SEM). The crystallographic structure was determined using the Anton Paar XRDynamic 500 powder diffractometer instrument. The surface area of the biomaterials was determined using the BELSORP-mini-X sorption analyser.

III. RESULTS

A. FTIR Results and Discussion:

The FTIR was employed to determine the chemical composition of the agro-waste and biochar sample by recording the infrared spectrum of the respective samples. The components of the sample can be identified by analyzing the spectra with relative intensities that represent different functional groups. All the FTIR results are discussed in reference to Table 1 which interprets the spectra for the Agilent Technologies FTIR analyser, which is the exact equipment that was used to conduct the FTIR analysis (Lakhmiri, 2017).

TABLE I: INTERPRETING SPECTRA FOR THE AGILENT TECHNOLOGIES FTIR ANALYSER [16, 17].

			Wavenumber			Wavenumber
Bond	Type of vibration		Range (cm ⁻¹)	Bond	Type of vibration	Range (cm ⁻¹)
C-H	Alkane	(Stretch)	3000 - 2850	C-O	Alcohols, esters,	
					ethers, Carboxylic	
	(-CH ₃)	(Bend)	1450 & 1375		acid, anhydrides	1300 - 1000
	(-CH ₂ -)	(Bend)	1465	О-Н	Alcohols, phenols	
	Alkene	(Stretch)	3100 - 3000		Free	3650 - 3600
			1000-650		H-Bonded	3400- 3200
	Aromatic	(Stretch)	3150-3050		Carboxylic acids	3400 - 2400
		(Out-of-		N-H	Primary &	
		plane bend)	900 - 600		secondary amines	
	Alkyne	(Stretch)	~3300		& amides (Stretch)	3500 - 3100
	Aldehyde		2900-2700		(bend)	1640 - 1550
C=C	Alkene		168 - 1600	C-N	Amines	1350 - 1000
	Aromatic		1600 & 1475	C=N	Imines & oximes	1690 - 1640
C≡C	Alkyne		2250 - 2100	C≡N	Nitriles	2260 - 2240
C=O	Aldehyde		1740 - 1720	N=O	Nitro (R-NO ₂)	1550 & 1350
	Ketone		1725 - 1705	S-H	Mercaptans	2550
	Carboxylix acid		1725 - 1700	C-X	Halides	
	Ester		1750 - 1730		Fluoride	1400 -1000
	Amide		1680 - 1630		Chloride	785 - 540
	Anhydride		1810 & 1760		Bromide, iodide	<650

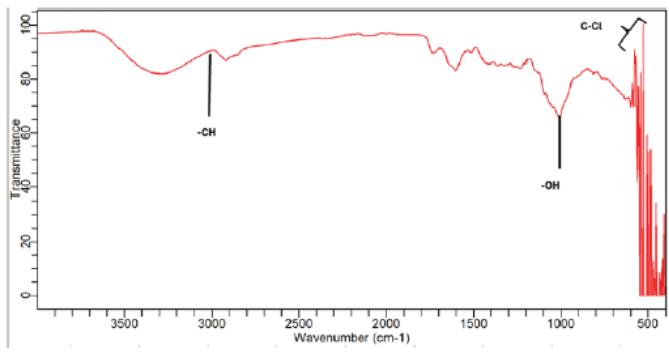


Fig. 2: FTIR spectrum for dry powdered orange peels

The peak observed around 2900 cm-1 is attributed to as a (-CH) stretching of the alkanes group. The peak around 1470 cm-1 of figure 3 above indicates the alkane bend. The bend observed around 1000 cm-1 in Figure 3 may indicate presence of the alkene group as well as alcohol (-OH) which tends to have affinity for heavy metals because of different charges [18]. The broad band stretching vibration of the hydroxyl (O-H) Functional group could be attributed to the adsorbed water in all organic materials [19]. The stretch of bends observed from around 650 cm-1 indicates the presence of the chloride group (C-Cl) [16].

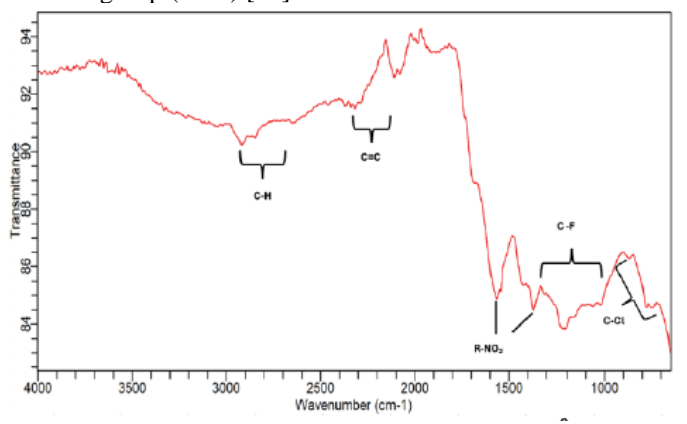


Fig. 3: FTIR for orange peels calcined 300 0C.

The multiple functional groups on calcined orange peel surfaces at 300 0C are shown in figure 4. The peaks observed around 2900 to 2700 cm-1 indicate the presence of aldehydes group (CH). The multiple peaks stretching from around 2300 to 2110 cm-1 indicates the presence of alkyne group (C C), according to table 1 above. Around 1550 and 1350 cm-1 sharp peaks can be observed which according to table 4.1.1 these two peaks indicate presence of nitro group (R-NO2). The peaks observed at around 1400 to 1000 cm-1 indicate the presence of fluoride group, and the peaks from around 770 to 590 cm-1 indicate the presence of chloride group which both groups are symbolized as C-Cl [16].

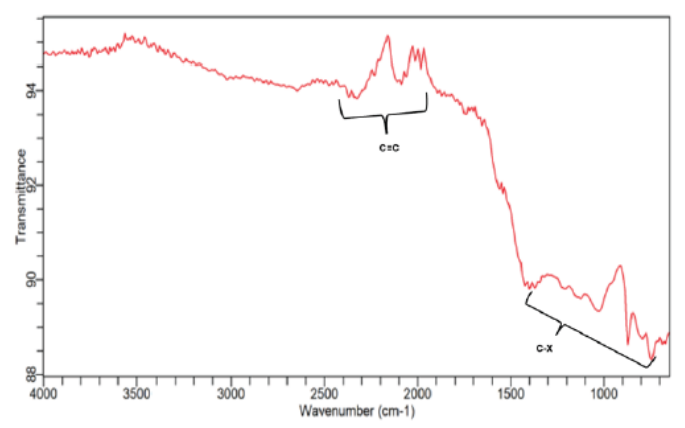


Fig. 4: FTIR for orange peels calcined 500 0C.

The multiple peaks stretching from around 2300 to 1900 cm-1 in figure 5 indicate the presence of the alkyne group (C C) which range between 2300 and 2100 cm-1 according to table 1. The multiple peaks that stretch from around 1400 to 500 cm-1 indicates the presence of fluorides (1400 to 1000 cm-1) and chlorides (785 to 540 cm-1) which are both symbolized as C-X [16]. The presence of C-X group on the surface of biochar tends to improve the affinity of heavy metals because of the difference of charges.

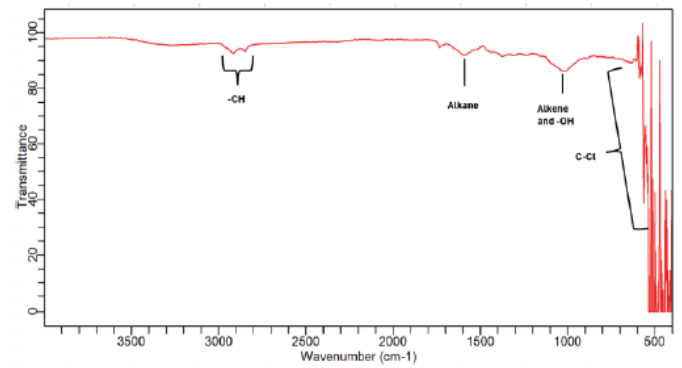


Fig. 5: FTIR for dry powdered banana peels

The out of a straight-line bend at observed around 2850 cm-1 can be recognized as the alkanes group (-CH). The peak around 1640 cm-1 of figure 6 above indicates the alkane bend. The end observed around 1000 cm-1 in figure 6 may indicate presence of the alkene group as well as alcohol (-OH). The stretch of bends observed from around 600 cm-1 indicates the presence of the chloride group (C-Cl). The presence of -OH and C-Cl groups (which are negatively charged) on the surface of the biochar may improve the affinity of heavy metals (which are positively charged) because of the difference of charges. The -OH functional group indication could be associated with the adsorbed water in all organic materials [16, 19].

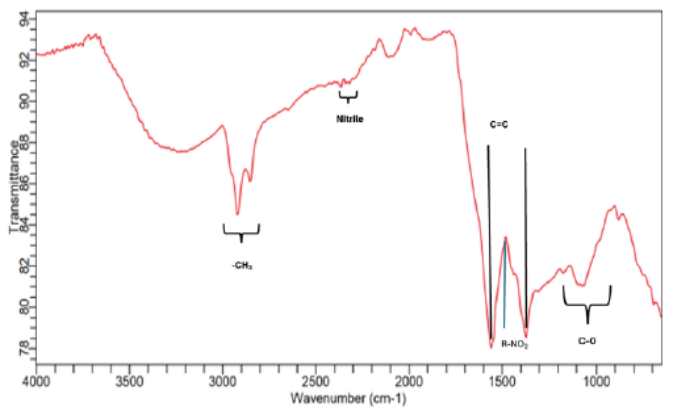


Fig. 6: FTIR for banana peels calcined 300 0C.

The stretch observed from around 3000 to 2820 cm-1 in figure 7 indicate the presence of alkanes (-CH3) on the 300 0C calcined banana peels surface. The peak around 2250 cm-1 indicates the presence of nitriles. The peaks at around 1570 and 1400 cm-1 indicate the presence of aromatic carbon structures (C=C). The peak observed around 1500 cm-1 indicates presence of nitro structures (R-NO2). The stretch from 1300 to 1000 cm-1 indicates the presence of alcohols, esters, ethers, carboxylic acid, and anhydrides- which are all have the general symbol CO [16]. The presence of C-O group on the surface of biochar may improve the affinity of heavy metals because of the difference of charges [18].

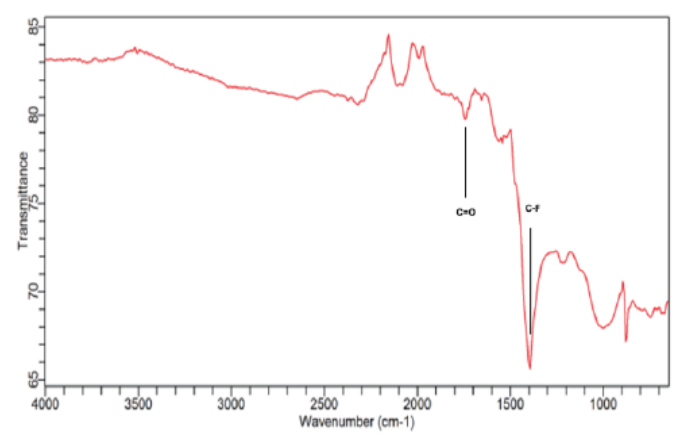


Fig 7: FTIR for banana peels calcined 500 0C.

The peak shown in figure 8 around 1760 cm-1 indicates the presence of the anhydride group (C=O). The peak at 1400 cm-1 indicates the presence of the fluoride group (C-F) [16]. The presence of C-F and C=O groups (which are negatively charged) on the surface of biochar tends to improve the affinity of heavy metals (generally positively charged) because of the difference of charges [18].

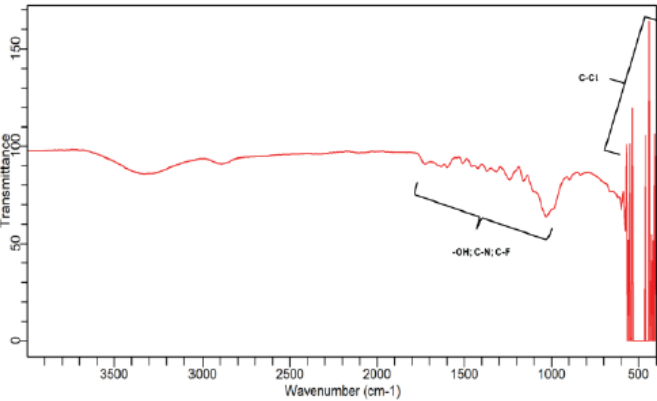


Fig.8: FTIR for dry sugar bagasse

The peak stretch from around 1600 to 1000 cm-1 of figure 9 above indicates the presence of alcohol (which stretch from 1300 to 1000 cm-1), amines (C-N, which stretch from 1350-1000 cm-1), and fluorides (C-F, which stretch from 1400 to 1000 cm-1). The bend observed around 1000 cm-1 in figure 9 may indicate presence of the alkene group as well as alcohol (-OH), this indication could be associated with the adsorbed water in all organic materials [16]. The stretch of bends observed from around 600 cm-1 indicates the presence of the chloride group (C-Cl). The presence of functional groups such as -OH, C-F, CN and C-Cl on the surface of biochar tends to improve the affinity of heavy metals because of the difference of charges.

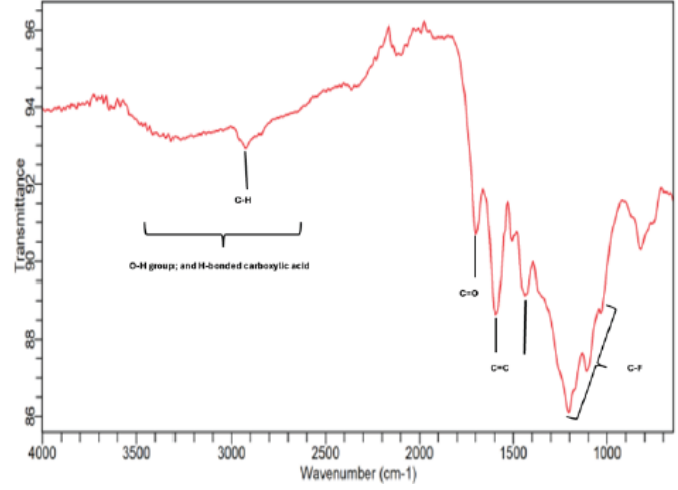


Fig. 9: FTIR Sugarcane bagasse calcined 300 0C.

The stretch from around 3500 up to 2400 cm-1 in figure 10 indicates the presence of the O-H group, specifically the Hbonded carboxylic acids. The peak around 2900 cm-1 indicates the presence of aldehydes (C-H). The peak around 1700 cm-1 indicates the presence of carboxylic acid (C=O). The peaks around 1600 and 1480 cm-1 indicates the presence of the aromatic group (C=C) [16]. The peaks stretching from 1300 to 1000 cm-1 indicates the presence of the fluoride group (C-F). The presence of functional groups such as C=O, and C-F on the surface of biochar may improve the affinity of heavy metals because of the difference of charges [18].

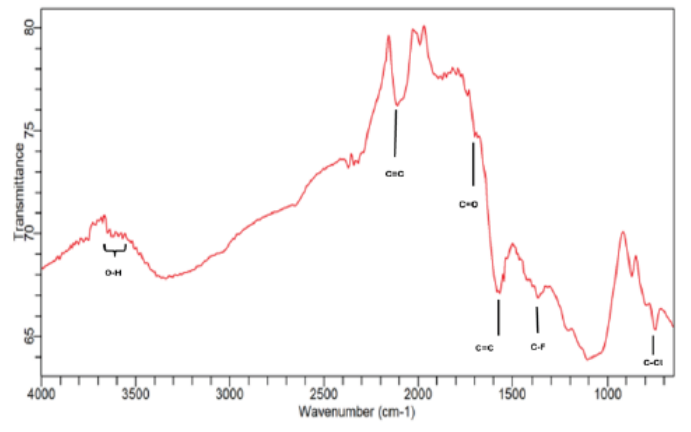


Fig. 10: FTIR Sugarcane bagasse calcined 500 0C.

The stretch shown in figure 11 from 3650 to 3600 cm-1 indicates the presence of alcohols and phenols (O-H), this indication could be associated with the adsorbed water in all organic materials [19]. The peak around 2200 cm-1 indicates the presence of alkyne (C C). The peak stretch around 1725 to 1700 cm-1 indicates the presence of carboxylic acid (C=O). The peak around 1600 cm-1 indicates the presence of the aromatic group (C=C) [16, 17]. The peak around 1400 cm-1 indicates the presence of the fluoride group (C-F). The peak around 780 cm-1 indicates the presence of chlorides (C-Cl).

XRD Results and Discussion:

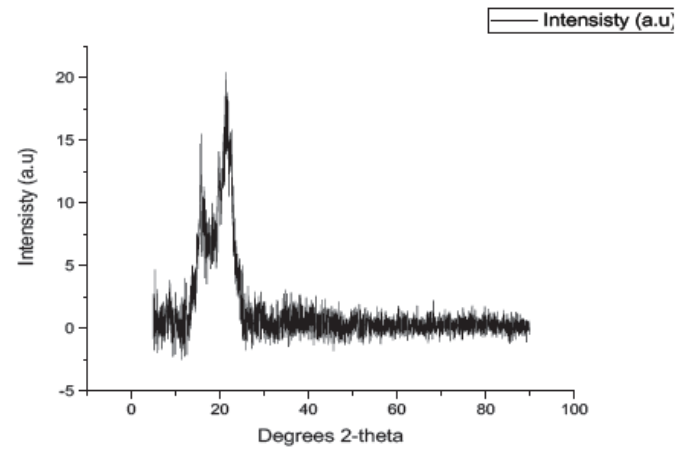


Fig. 11: XRD Results of dried orange peels.

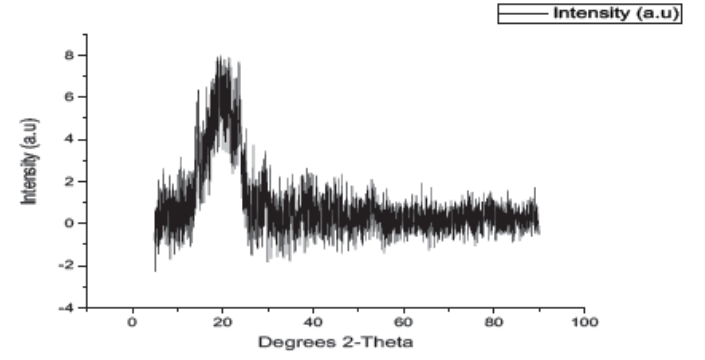


Fig.12: XRD Results for calcined orange peels at 300 0C.

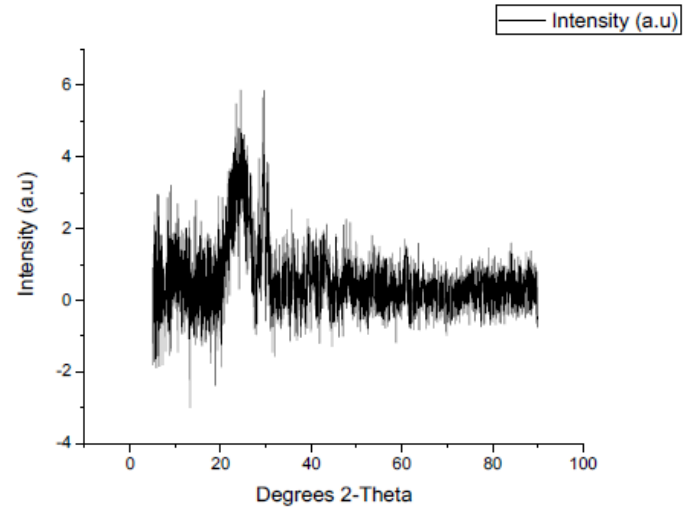


Fig. 13: XRD Results for calcined orange peels at 500 0C.

Figure 12 show two key fractions at $2\theta=160$ and 220 corresponding with 15 and 23 characteristic crystal planes of graphite respectively. The trend for figures 13 and 14 are broadened, indicating poor crystallinity and amorphousness. Figure 4.18 shows a singular peak at $2\theta=200$ corresponding with 8 crystal planes. The peaks for figure 14 are unclear, however three fractions at $2\theta=100$, 280 and 320 corresponding to 2.2, 2.7 and 3.7 for figure 13, and 3, 5.8 and 6 for figure 14 characteristic crystal planes respectively.

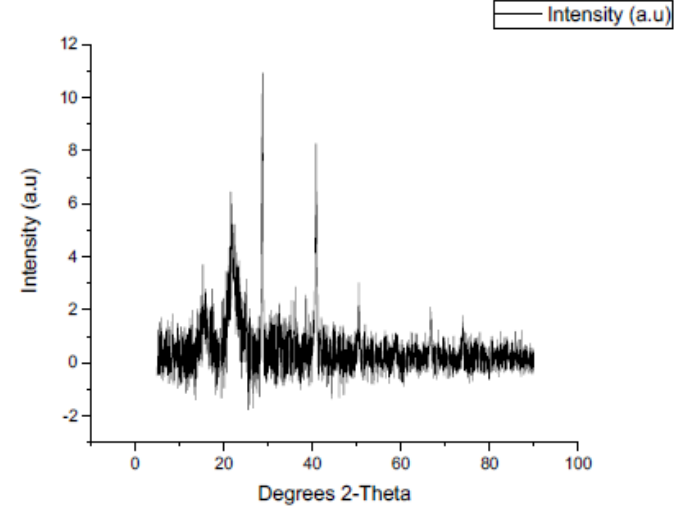


Fig. 14: XRD dried banana peels.

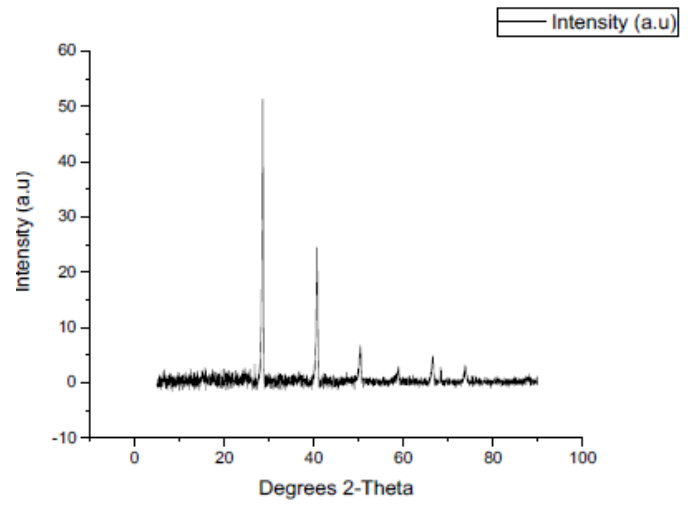


Fig. 15: XRD Results for calcined banana peels 300 0C.

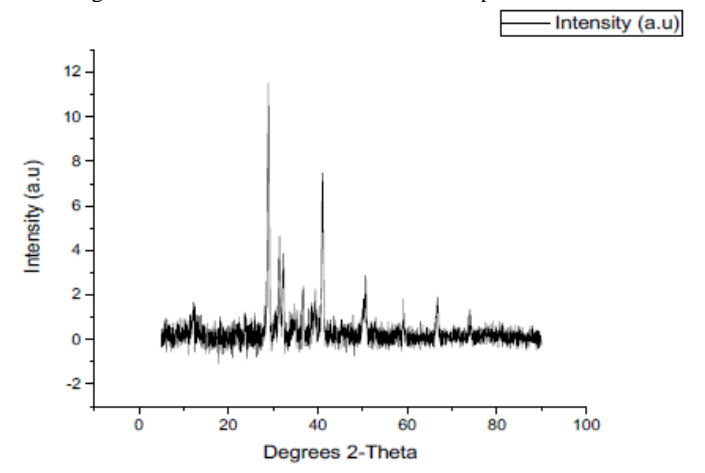


Fig. 16: XRD Results for calcined banana peels 500 0C.

Figure 15 shows five key fractions at $2\theta = 160$, 220, 280, 420, and 510 corresponding with intensities of 3, 6, 11, 8, and 3 characteristic crystal planes of graphite respectively. Figure 16 shows six peaks at $2\theta = 280$, 400, 500, 580, 670, 740 corresponding with 51, 25, 6, 3, 5, and 4 crystal planes of graphite respectively. The peaks for figure 17 show very similar trends in that they both have six clear trends fractions at $2\theta = 290$, 320, 420, 500, 670, and 750 corresponding to 12, 4, 6, 2, 2, and 1 characteristic crystal planes of graphite respectively.

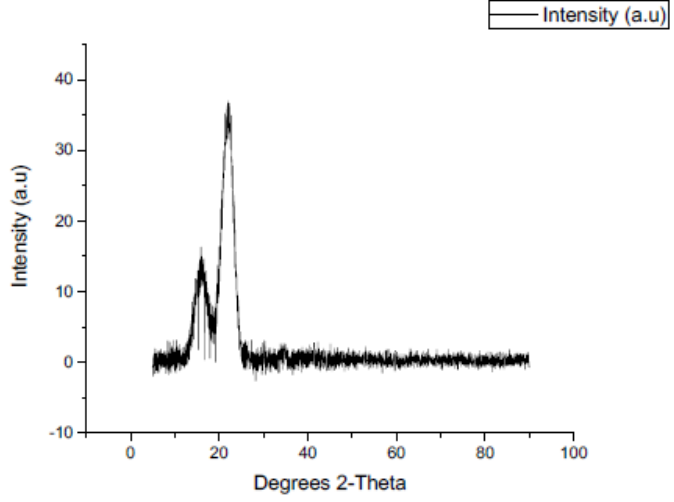


Fig. 17: XRD dried sugarcane bagasse.

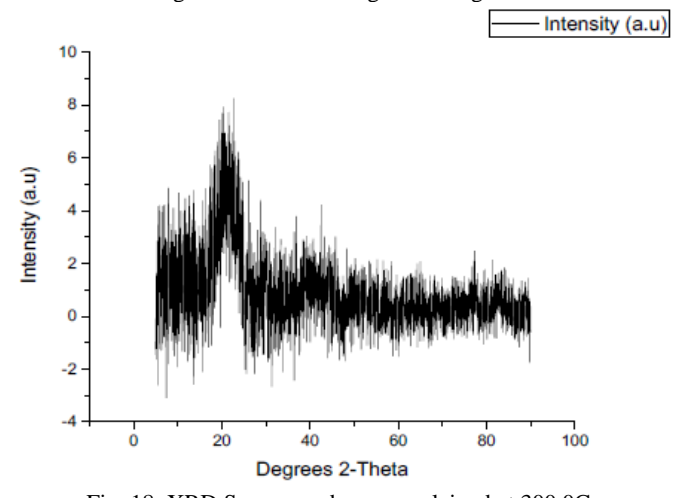


Fig. 18: XRD Sugarcane bagasse calcined at 300 0C.

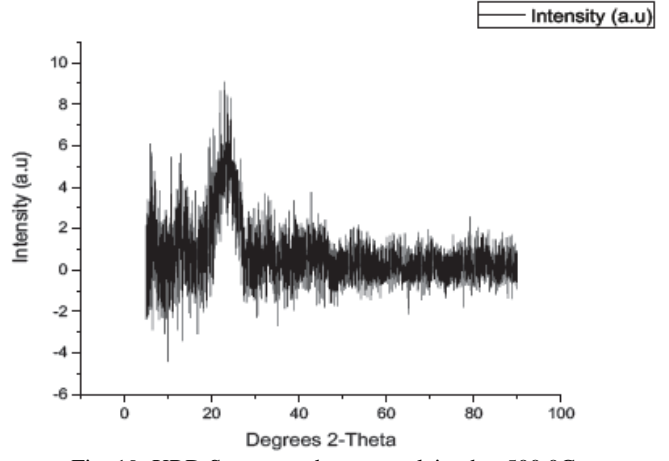
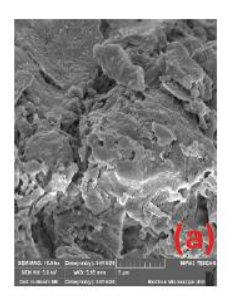
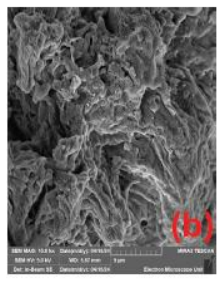


Fig. 19: XRD Sugarcane bagasse calcined at 500 0C.

From figures 18 trends two key fractions at $2\theta = 160$ and 220 corresponding with 16 and 36 can be observed. The trend for figures 19 and 20 are broadened, indicating poor crystallinity and amorphousness. Figure 4.28 shows a singular peak at $2\theta = 200$ corresponding with 8 crystal planes. The peaks for figure 4.30 are also singular and they both show a fraction at $2\theta = 230$ corresponding to 9 characteristic crystal planes.

B. SEM Results and Discussion:





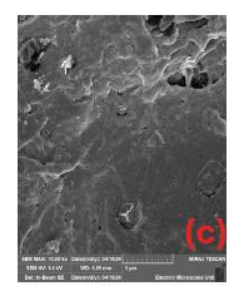
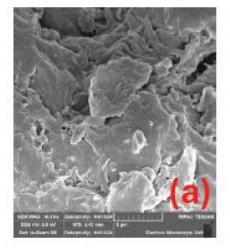


Fig. 20: (a) Dried orange peels SEM micrographs. (b) Calcined orange peels at 300 OC SEM micrographs. (c) Calcined orange peels at 500 OC SEM micrographs.

The dry powdered orange peels Scanning Electron Microscopy (SEM) results depicted in figure 20 (a) shows the porous structures which indicate increased surface area for adsorption sites. It can be observed that as the temperature of calcination increases so does the porousness increase in both figures 20 (b) and (c) this is evident. Thus, meaning that the surface area is increased as the temperature of calcination increases.





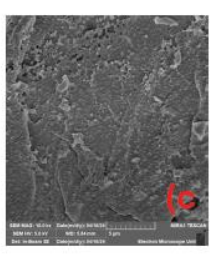
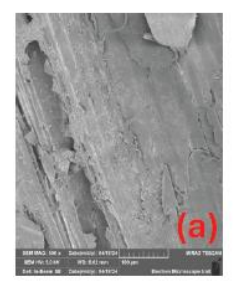
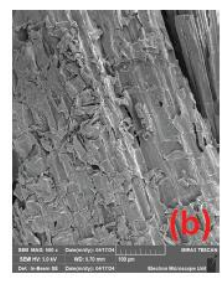


Fig. 21: (a) Dried banana peels SEM micrographs at different magnitudes. (b) Calcined banana peels at 300 0C SEM micrographs at different magnitudes. (c) Calcined banana peels at 500 0C SEM micrographs at different magnitudes.

The dry powdered banana peels SEM images depicted in figure 21 (a) shows the porous structures which indicate increased surface area thus increased adsorption sites. Figures 21 (a) and (b) show the SEM images for the calcined banana peels at temperatures 300 0C and 500 0C, respectively. It can be observed that as the temperature of calcination increases so does the porousness increase. An increase in the porous size means an increase in the adsorption sites.





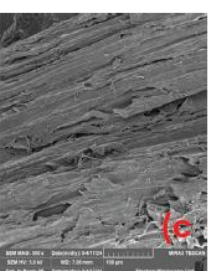


Fig. 22: (a) Dried sugarcane bagasse SEM micrographs at different magnitudes. (b) Calcined sugarcane bagasse at 300 0C SEM micrographs at different magnitudes. (c) Calcined sugarcane bagasse at 500 0C SEM micrographs at different magnitudes.

The SEM images depicted in figure 22 (a) shows the porousness of dry sugarcane bagasse, which shows they can be

used adsorption. However, it can be observed from figures (b) and (c) that as the temperature of calcination increases so does the porousness also increase. Indicating that increasing the temperature of calcination increases the adsorption sites.

IV. CONCLUSION

The characterization qualities of the biochar were studied using FTIR, XRD, and SEM. These characterization results obtained almost all showed a common trend, that is as the temperature of calcination so does the quality of the absorptivity of the biochar increase. The peak stretch around 1725 to 1700 cm-1 (shown in figure 11) indicated the presence of carboxylic acid (C=O), thus making sugarcane a more desirable agro-waste material for further studies. For XRD results it was discovered that characteristic crystal planes of graphite respectively, which again make sugarcane bagasse a desirable agro-waste material for water treatment. An interesting observation made was that the structure of orange peels calcined at 300 OC (figure 22) seems to be more porous, which is a desirable trait for biosorbent application.

V. ACKNOWLEDGMENT

I would like to express my gratitude to my supervisors for their unfailing assistance in the preparation of this paper.

REFERENCES

- [1] Liu, X.-Y., et al., Microalgae-based swine wastewater treatment: Strain screening, conditions optimization, physiological activity and biomass potential. Science of The Total Environment, 2022. 807: p.151008.
 - https://doi.org/10.1016/j.scitotenv.2021.151008
- [2] Gautam, R.K., et al., Contamination of heavy metals in aquatic media: transport, toxicity and technologies for remediation. 2014. https://doi.org/10.1039/9781782620174-00001
- [3] Saravanan, A., et al., Mixed biosorbent of agro waste and bacterial biomass for the separation of Pb (II) ions from water system. Chemosphere, 2021. 277: p. 130236. https://doi.org/10.1016/j.chemosphere.2021.130236
- [4] Topare, N.S. and V.S. Wadgaonkar, A review on application of lowcost adsorbents for heavy metals removal from wastewater. Materials Today: Proceedings, 2023. 77: p. 8-18. https://doi.org/10.1016/j.matpr.2022.08.450
- [5] Zhang, W., et al., Sorbent properties of orange peel-based biochar for different pollutants in water. Processes, 2022. 10(5): p. 856. https://doi.org/10.3390/pr10050856
- [6] Hussain, A., S. Madan, and R. Madan, Removal of heavy metals from wastewater by adsorption. Heavy metals—Their environmental impacts and mitigation, 2021. https://doi.org/10.5772/intechopen.95841
- [7] Rajendran, S., et al., A critical and recent developments on adsorption technique for removal of heavy metals from wastewater-A review. Chemosphere, 2022. 303: p. 135146. https://doi.org/10.1016/j.chemosphere.2022.135146
- [8] Zaimee, M.Z.A., M.S. Sarjadi, and M.L. Rahman, Heavy metals removal from water by efficient adsorbents. Water, 2021. 13(19): p. 2659.
 - https://doi.org/10.3390/w13192659
- [9] Faber, M., R. Laubscher, and S. Laurie, Availability of, access to and consumption of fruits and vegetables in a periurban area in KwaZuluNatal, South Africa. Maternal & Child Nutrition, 2013. 9(3): p. 409-424. https://doi.org/10.1111/j.1740-8709.2011.00372.x
- [10] Raji, I.A. and C.T. Downs, Fruiting phenology and diversity of native Ficus species in an urban forest mosaic landscape in KwaZuluNatal,

- South Africa. African Journal of Ecology, 2022. 60(4): p. 1357-1357-1362.
- https://doi.org/10.1111/aje.13017
- [11] Nagendran, R. Agricultural waste and pollution. in Waste. 2011. Elsevier.
 - https://doi.org/10.1016/B978-0-12-381475-3.10024-5
- [12] Gita, S., et al., Adsorption-biodegradation coupled remediation process for the efficient removal of a textile dye through chemically functionalized sugarcane bagasse. Water Environment Research, 2021. 93(10): p. 2223-2236. https://doi.org/10.1002/wer.1595
- [13] Castilla-Caballero, D., et al., Effect of pyrolysis, impregnation, and alcination conditions on the physicochemical properties of TiO2/Biochar composites intended for photocatalytic applications. Journal of Environmental Chemical Engineering, 2023. 11(3): p. 110274.
 - https://doi.org/10.1016/j.jece.2023.110274
- [14] Wang, M., H. Zhou, and F. Wang, Photocatalytic production of syngas from biomass. Accounts of Chemical Research, 2023. 56(9): p. 1057-1069.
 - https://doi.org/10.1021/acs.accounts.3c00039
- [15] Göransson, K., et al., Review of syngas production via biomass DFBGs. Renewable and Sustainable Energy Reviews, 2011. 15(1): p. 482-492.
 - https://doi.org/10.1016/j.rser.2010.09.032
- [16] Berthomieu, C. and R. Hienerwadel, Fourier transform infrared (FTIR) spectroscopy. Photosynthesis research, 2009. 101: p. 157-170. https://doi.org/10.1007/s11120-009-9439-x
- [17] Nandiyanto, A.B.D., R. Oktiani, and R. Ragadhita, How to read and interpret FTIR spectroscope of organic material. Indonesian Journal of Science and Technology, 2019. 4(1): p. 97-118. https://doi.org/10.17509/ijost.v4i1.15806
- [18] Salem, I.B., et al., Date palm waste pyrolysis into biochar for carbon dioxide adsorption. Energy Reports, 2021. 7: p. 152-159. https://doi.org/10.1016/j.egyr.2021.06.027
- [19] Mujtaba, G., et al., Physio-chemical characterization of biochar, compost and co-composted biochar derived from green waste. Sustainability, 2021. 13(9): p. 4628. https://doi.org/10.3390/su13094628